AD

TECHNICAL REPORT ARCCB-TR-99020

# X-RAY DIFFRACTION TECHNIQUES AND FINITE ELEMENT MODELING TO CONTROL RESIDUAL STRESS IN HIGH-TEMPERATURE PRESSURE VESSELS

S. L. LEE
M. LEACH
P. CHEN
P. COTE
D. WINDOVER

NOVEMBER 1999

US ARMY ARMAMENT RESEARCH,
DEVELOPMENT AND ENGINEERING CENTER
CLOSE COMBAT ARMAMENTS CENTER
BENÉT LABORATORIES
WATERVLIET, N.Y. 12189-4050

APPROVED FOR PUBLIC RELEASE; DISTRIBUTION UNLIMITED

## DISCLAIMER

The findings in this report are not to be construed as an official Department of the Army position unless so designated by other authorized documents.

The use of trade name(s) and/or manufacturer(s) does not constitute an official endorsement or approval.

## DESTRUCTION NOTICE

For classified documents, follow the procedures in DoD 5200.22-M, Industrial Security Manual, Section II-19, or DoD 5200.1-R, Information Security Program Regulation, Chapter IX.

For unclassified, limited documents, destroy by any method that will prevent disclosure of contents or reconstruction of the document.

For unclassified, unlimited documents, destroy when the report is no longer needed. Do not return it to the originator.

# REPORT DOCUMENTATION PAGE

Form Approved
OMB No. 0704-0188



| 1. AGENCY USE ONLY (Leave blank) | 2. REPORT DATE | 3. REPORT TYPE AND DATES COVERED |
|---|---|---|
| | November 1999 | Final |

**4. TITLE AND SUBTITLE**

X-RAY DIFFRACTION TECHNIQUES AND FINITE ELEMENT MODELING TO CONTROL RESIDUAL STRESS IN HIGH-TEMPERATURE PRESSURE VESSELS

**5. FUNDING NUMBERS**

AMCMS No. 6111.01.91A1.1

**6. AUTHOR(S)**

S.L. Lee, P. Chen, M. Leach, P. Cote, and D. Windover

**7. PERFORMING ORGANIZATION NAME(S) AND ADDRESS(ES)**

U.S. Army ARDEC
Benet Laboratories, AMSTA-AR-CCB-O
Watervliet, NY 12189-4050

**8. PERFORMING ORGANIZATION REPORT NUMBER**

ARCCB-TR-99020

**9. SPONSORING/MONITORING AGENCY NAME(S) AND ADDRESS(ES)**

U.S. Army ARDEC
Close Combat Armaments Center
Picatinny Arsenal, NJ 07806-5000

**10. SPONSORING/MONITORING AGENCY REPORT NUMBER**

**11. SUPPLEMENTARY NOTES**

Presented at the 1999 Society for Experimental Mechanics Conference, Cleveland, OH, 7-9 June 1999.
Published in proceedings of the conference.

**12a. DISTRIBUTION/AVAILABILITY STATEMENT**

Approved for public release; distribution unlimited.

**12b. DISTRIBUTION CODE**

**13. ABSTRACT** *(Maximum 200 words)*

Manufacturing operations, such as swage autofrettage, shot peening, and overload processes, have been used to impart advantageous residual stresses to improve fatigue life in components used in high-temperature pressure vessels. Both experimental and modeling techniques depend on the geometry and processing history of the component under investigation. This report compares x-ray diffraction residual stress measurements in a swage autofrettaged steel cylinder with finite element modeling results of a cylinder with a given bore expansion. The report also examines an analytical model of a cylinder under internal pressure, including both Bauschinger and strain-hardening effects. From a simple swaged cylinder to a complicated perforated cylinder and overstrained and shot-peened multiple-lug breech structure, control of residual stresses through experimental and modeling efforts is vital in the design of pressure vessels. This report discusses the role of slicing operations, surface polishing, surface roughness, and resolution effects in structures that contain high stress gradients.

**14. SUBJECT TERMS**

Pressure Vessels, Residual Stress, Surface Roughness Effect, Surface Polishing Effect, Surface Stress Gradients, Slicing Effect

**15. NUMBER OF PAGES**

19

**16. PRICE CODE**

| 17. SECURITY CLASSIFICATION OF REPORT | 18. SECURITY CLASSIFICATION OF THIS PAGE | 19. SECURITY CLASSIFICATION OF ABSTRACT | 20. LIMITATION OF ABSTRACT |
|---|---|---|---|
| UNCLASSIFIED | UNCLASSIFIED | UNCLASSIFIED | UL |

## TABLE OF CONTENTS



### TABLES



### LIST OF ILLUSTRATIONS

## INTRODUCTION

Residual stress control plays an important role in the development of components for high-temperature pressure vessels, and its attainment requires a coherent experimental and modeling effort. The swage autofrettage process is known to generate favorable residual stresses in the walls of a cylinder to enhance fatigue life (refs 1,2). However, x-ray diffraction measurements taken from the surfaces of the polished cross sections of the cylinder deviated from Tresca's model predictions of residual stresses for a cylinder under internal pressure and O'Hara's finite element swage model (refs 3,4). To help interpret the reduced compressive residual stresses observed near the bore, Chen's analytic model of a cylinder under internal pressure included Bauschinger and strain-hardening effects (ref 5). Parker and Underwood further compared various modeling results and disclosed that the ASME pressure vessel code does not predict the experimentally-observed reduced compressive stresses near the bore (ref 6). In this work, a cylinder with inner diameter (ID) of 113.8-mm, outer diameter (OD) of 304.8-mm, and OD/ID of 2.67 was autofrettaged to give a radial expansion of 1.38-mm. X-ray residual stress measurements were compared with a finite element model and an analytical model of a cylinder under internal pressure taking into effect the Bauschinger factor and strain hardening.

Residual stress analyses of a shot-peened and overload multi-lug breech ring (refs 7,8), and of a swaged perforated cylinder (refs 9-11) have been reported. A review of the results is presented here in light of changing experimental and modeling strategies due to specimen geometry, processing history, and expected stress distribution. A short-range stress depth profile from the lugs of the peened breech ring was studied by successive x-ray measurements, layer-by-layer material removal from the inside surfaces of the lug, and correction for relaxation due to layer removal. Long-range location-dependent overload residual stresses were measured on the cross-section slices. In the perforated cylinder, finite element modeling predicted a high gradient stress component (ref 9). This prompted the simulation of resolution effects on stress measurements in distributions containing high stress gradients. Optimized spatial resolution was used to achieve improved agreement with finite element modeling results near the root of the perforations.

Because of the limitation of x-ray penetration, residual stress measurements are generally taken from the cross-section slices. Effects of the slicing operation are discussed by comparing the finite element model before and after slicing. Surface material removal by electropolishing is common in x-ray stress analysis. This is to remove effects due to machining and oxidation, which may affect stress measurements. Li et al. (ref 12) reported that when surface roughness approaches the depth of x-ray penetration, residual stress levels are reduced. They examined laser confocal microscope images of steel surfaces after mild and aggressive electropolishing and etching processes. Their study demonstrated that rough surfaces exceeding 75% chromium x-ray penetration depth resulted from improper processing.

## X-RAY EXPERIMENTAL TECHNIQUES

Our residual stress measurements were performed on a Ω-tilt stress analyzer using the [211] reflection from 4340 steel at 156.41° two-theta. Chromium radiation and a position-sensitive proportional counter were used for stress analysis. Cross-sectional slices of 25 to 38-mm thicknesses were cut from the 120-mm cylinder after the swage operation. The slices were machine-polished, and 125 to 250 μm material was removed from the surface by electropolishing. The electropolishing procedure was performed using 50% of $H_3PO_4$, 25 % $H_2SO_4$, and 25% $H_2O$ solution in a large flow-through tank at Watervliet Arsenal. An alternative material removal method using 85% $H_2O$, 7 to 10% hydrogen fluoride (HF), and 15% hydrogen peroxide etch was tested. This method of material removal had been suggested earlier by the consortium of the National Center for Manufacturing Sciences (NCMS) to measure stresses in predictive heat-treatment studies of automotive gear (ref 13). For measurements of depth profiles, such as in the lugs of the shot-peened breech, an additional reference MTI bench micrometer was used to monitor thickness of material removed.

## EXPERIMENTAL RESIDUAL STRESS IN A 120-MM M256 SWAGE AUTOFRETTAGED CYLINDER

Figure 1a is a schematic of the swage autofrettage process. An oversized mandrel is pushed through the interior walls of the cylinder to produce yield zones near the bore. X-ray residual stress measurements were taken from a 25.4-mm thick slice. Figure 1b shows the stress distribution as a function of radial distance from the bore. The figure shows hoop stresses along the 0° direction, averaged hoop stresses from the 0°, 90°, 180°, and 270° directions, radial stresses along 0°, and averaged radial stresses from 0° and 180°. X-ray measurements disclosed compressive stresses near the ID, changing to tensile stresses near the OD. Reduced residual stresses were observed near the bore. From the contour of the distribution, we conclude that the reverse yielding zone extends from 60 to 73-mm, the plastic deformation zone from 73 to 110-mm, and the elastic zone from 110 to 152-mm radial distances from the center of the cylinder. The percentage overstrain extracted from the curve was approximately 70%.

## COMPARISON OF EXPERIMENTAL AND FINITE ELEMENT MODEL OF THE 120-MM M256 AND EFFECT OF SLICING

The elastic-plastic finite element model considers the strain-hardening effect of the material and uses the generalized plane-strain elements of the ABAQUS finite element program (ref 14). These special elements with nonzero axial strains are useful for modeling the autofrettage process due to swaging. We used 20 ten-node biquadratic generalized plane-strain quadrilateral elements and 289 nodes, taking full advantage of symmetries. We also used a simple isotropic hardening rule with an initial yield stress of 1116 MPa and the ratio of tangent modulus to Young's modulus, m = 0.5%. The nonlinear finite element modeling consisted of several steps including the autofrettage process simulated by forced radial displacement and relaxation of autofrettage. Finally, multi-point constraint equations were used to conform the element formulation into a plane-stress condition consistent with the sliced specimens used for x-ray biaxial stress analysis.

Figure 1c depicts the mesh of 20-axisymmetric elements with 8-nodes each used in the ABAQUS finite element model. Figure 1d depicts the hoop stresses during and after autofrettage, and the effect of slicing on hoop stresses. Little stress relaxation, especially near the bore, is predicted due to the slicing operation.

Figure 1e compares experimental stress measurements with the ABAQUS modeling results. Predicted stresses deviated from the experimental stress distribution, especially near the bore region. Also shown in Figure 1e are two results with and without combined Bauschinger and hardening effects from an analytic model (ref 15), in comparison with experimental averaged hoop stresses. Reverse yielding occurs in all cases near the bore. The finite element model results after slicing and analytical results based on a simple isotropic hardening rule are in excellent agreement. The results showing the combined Bauschinger and hardening effects are based on $m = 0.005$, $m' = 0.3$, and variable f (Bauschinger effect factor) determined in the program as a function of plastic strain. The combined Bauschinger and hardening effects cause a larger reverse yielding zone and a smaller compressive hoop stress near the bore. Thus, a better agreement between the modeling and measurement is achieved.

Figure 1f shows the radial residual distributions based on two finite element models, two analytical models, and the averaged data based on x-ray diffraction. Figure 1c shows that the slicing operation reduces compressive stresses by a maximum of 150 MPa near the bore. The slicing effect on hoop stresses should be a fraction of the maximum deviation due to the finite thickness of the slice. Deviation should decrease with increasing thickness of the slice.

## MEASUREMENT OF OVERLOAD AND SHOT PEENING STRESSES IN AN EX35 BREECH RING

Figure 2a shows geometry of the multi-lug breech superimposed on the finite element mesh (refs 7,8). The breech ring is on the top showing the front (right), middle, and rear lugs. The breech block is shown on the bottom with applied pressure acting from the right. Shot peening of the breech ring lugs was performed at Hydro Honing Lab, and the overload operation of the breech ring was performed at Benét labs. Shot-peen stresses on the surfaces of the lugs were studied, as well as overload stresses on the cross sections.

Figure 2b shows the hoop and axial peening stresses in the middle lug. Figure 2c shows the hoop and radial stress distributions along a vertical direction beneath the front and middle lugs. X-ray results concluded that compressive stresses generated in the lugs by the two methods were of similar magnitude, but depth of the overload stresses extended an order of magnitude deeper than the peening stresses. The short-ranged peening stresses in the new breech design resulted in 13,589 cycles fatigue test-to-failure. The long-ranged overload stresses resulted in 26,553 cycles-to-failure for the component (ref 8).

## STRESSES IN A SWAGED PERFORATED CYLINDER AND EFFECTS OF HIGH STRESS GRADIENTS AND SLICING

Figure 3a presents a section of the perforated cylinder with superimposed finite element mesh (ref 11). Figure 3b presents Parker's predicted hoop stress distribution from bore to perforation (ref 9). The high stress gradients near the root of the perforation prompted our simulation of resolution effect using five-point averaging, which corresponded to 2.0-mm lateral resolution. Experimental measurements were performed using an optimized collimator and slit to improve stress results near the bore and at the perforations.

Figure 3c shows the ABAQUS stresses by applying a bore pressure of 434 MPa and measured hoop residual stresses from bore to perforation. From the resultant stress levels, the bore and the root of the perforation are competing locations for failure. Failure should occur at the root of the perforation judged by the higher tensile stress levels at the root compared to the bore. Fatigue test results verified the prediction from experimental results. In comparing Figures 3b and 3c, the finite element model predicted much greater compressive residual stress levels near the root of the perforation compared to experimental measurements. Inside-diameter peening of the perforations is suggested to further improve fatigue life in this component.

Figure 3d shows the ABACUS hoop residual stress using plane-stress and generalized plane-strain. The plane-stress results simulate the slicing operation. Hoop stress distributions are very similar.

## SURFACE ROUGHNESS EFFECT ON STRESS MEASUREMENT

Li et al. (ref 12) have examined the effect of surface roughness on x-ray diffraction stress measurement. In their study, steel surfaces were machined to induce roughness, and then tempered in vacuum at 600°C for 15 hours to minimize the effect on residual stress due to machining. They concluded that roughness reduces the stress levels when it is comparable to the depth of x-ray penetration.

Figure 4a depicts the effect of specimen surface roughness on x-ray penetration. The top graph shows the case when the surface roughness is less than the x-ray penetration. The bottom shows when the surface roughness is greater than the x-ray penetration depth. When the surface is rough, there would be more stress relaxation in the crest region, and stress concentration in the valley region. Shadowing effect, specimen surface curvature, beam diameter, surface inclination, and integration effect can affect x-ray stress measurements (ref 16). Figure 4b depicts the ratio of x-ray-measured stresses to the implied stresses as a function of roughness.

X-ray penetration depends on the wavelength of x-ray and the diffraction angle used for stress measurements. Table 1 gives the depth of x-ray penetration in gun steel (94.5% iron, 2.85% nickel, 1% chromium, and 0.5% molybdenum). In the table, $\mu/\rho$ gives the mass absorption coefficients in ($cm^2/g$), $\rho$ gives density in $g/cm^3$, and T represents the fractional percentage of x-ray beam not being absorbed, which contributes to the diffraction peak. Using chromium K-$\alpha$ radiation, and the [211] reflection from steel at 156.41° two-theta, x-ray

penetration is ~11 to 16 μ for 95% penetration, and ~2 to 4 μ for 50% penetration. Figure 4b shows that when roughness exceeds 20 μ, residual stress measurement by the x-ray method falls.

## EFFECT OF POLISHING ON SURFACE ROUGHNESS

A laser confocal microscope was used to examine steel surfaces before and after electropolishing and etching operations. Figure 5a gives the perspective of a steel specimen after polishing with diamond, and removal of 25 μm of surface material using perchloric acid. The figure shows surface roughness of 1 to 2 μm. Figure 5b shows a steel specimen surface that was aggressively etched using HF and hydrogen peroxide mixture. This figure shows extensive surface irregularities and roughness. The polishing technique should be optimized to provide minimum surface roughness and stress modifications for x-ray residual stress measurement.

## REFERENCES


1. Davidson, T.E., Kendall, D.P., and Reiner, A.N., "Residual Stresses in Thick-Walled Cylinders Resulting from Mechanical Induced Overstrain," Technical Report WVT-6319, Watervliet Arsenal, Watervliet, NY, 1963.

2. Davidson, T.E., Throop, J.F., Reiner, A.N., and Austin, B.A., "Analysis of the Effect of Autofrettage on the Fatigue Life Characteristics of the 175-mm M113 Gun Tube," Technical Report WVT-6901, Watervliet Arsenal, Watervliet, NY, 1969.

3. Lee, S.L., O'Hara, G.P., Olmstead, V., and Capsimalis, G., "Characterization of Residual Stresses in an Eccentric Swage Autofrettaged Thick-Walled Steel Cylinder," *Proceedings of ASM International Conference on Practical Applications of Residual Stress Technology*, 1991, pp. 123-129.

4. Lee, S.L., Britt, L., and Capsimalis, G., "Comparison of Residual Stress and Hardness in a Symmetric and Eccentric Swage Autofrettaged Cylinder," *Nondestructive Characterization of Materials VI*, Plenum Press, 1994, pp. 425-434.

5. Chen, P.C.T., "The Bauschinger and Hardening Effects on Residual Stresses in an Autofrettaged Thick-Walled Cylinder," *Trans. ASME, Journal of Pressure Vessel Technology*, Vol. 108, 1986, pp. 108-112.

6. Parker, A.P., and Underwood, J.H., "The Bauschinger Effect - A comparison of Relevant Sections of the ASME Pressure Vessel Code," *Journal of Pressure Vessel Technology*, 1999.

7. Lee, S.L., Glennon, M.J., and Gabriele, A., "Induced Overload Residual Stresses in EX35 Multi-Lug Breech Ring," Technical Report ARCCB-TR-95036, Benet Laboratories, Watervliet, NY, August 1995.

8. Lee, S.L., and Scavullo, M., "Effect of Shot Peening and Overload Residual Stresses on EX35 Multi-Lug Breech Fatigue Life," Technical Report ARCCB-TR-96028, Benet Laboratories, Watervliet, NY, September 1996.

9. Parker, A.P., Endersby, S.N., Bond, T.J., Underwood, J.H., Lee, S.L., and Higgins, J., "Stress Concentration, Stress Intensity, and Fatigue Lifetime Calculations in Autofrettaged Tubes Containing Axial Perforations Within the Wall," *Trans. ASME, Journal of Pressure Vessel Technology,* Vol. 119, 1997, pp. 488-493.

10. Lee, S.L., Hyland, E., Neese, J., and Windover, D., "Residual Stress in a Swage Autofrettaged Steel Cylinder with Semi-Circular Mid-Wall Channels," *Proceedings of the 1997 SEM Spring Conference on Experimental and Applied Mechanics*, pp. 121-126.

11. Chen, P.C.T., Leach, M., and Lee, S.L., "Modeling and Measurement of Residual Stresses in a Swage Autofrettaged Cylinder with Axial Perforations," *Proceedings of the 1998 SEM Spring Conference on Experimental and Applied Mechanics*, p. 423.

12. Li, A., Ji, V., Lebrun, J.L., and Ingelbert, G., "Surface Roughness Effects on Stress Determination by the X-Ray Diffraction Method," *SEM Experimental Techniques*, 1995, pp. 9-11.

13. "Predictive Model and Methodology for Heat Treatment Distortion Phase 1A Demo," National Center for Manufacturing Sciences, Cleveland, OH, 27 September 1994.

14. *ABAQUS/Standard User's Manual*, Version 5.7, Hibbitt, Karlsson, and Sorensen, Inc., 1997.

15. Chen, P.C.T., "Stress and Deformation Analysis of Autofrettaged High Pressure Vessels," *ASME Pressure Vessels and Piping Conference*, PVP Vol. 110, 1986, pp. 61-67.

16. Goldenbogen, S., Weile, K.H., Krause, F., Kampfe, B., and Skurt, L., *Proceedings of Third European Conference on Residual Stresses*, Frankfort, November 1992, pp. 433-438.

**Table 1. X-Ray Penetration in A723 Gun Steel**

| Element | μ/ρ | Percentage | Mass Fraction | Atomic Weight | Density |
|---|---|---|---|---|---|
| Iron | 113.100 | 94.474 | 0.9439 | 55.8470 | 7.8700 |
| Nickel | 145.700 | 2.850 | 0.0299 | 58.7100 | 8.9100 |
| Chromium | 85.710 | 1.000 | 0.0093 | 51.9960 | 7.1900 |
| Manganese | 96.080 | 0.600 | 0.0059 | 54.9380 | 7.4700 |
| Molybdenum | 457.400 | 0.500 | 0.0086 | 95.9400 | 10.2200 |
| Carbon | 14.460 | 0.340 | 0.0007 | 12.0110 | 2.2700 |
| Silicon | 202.700 | 0.125 | 0.0006 | 28.0860 | 2.3300 |
| Vanadium | 75.060 | 0.105 | 0.0010 | 50.9414 | 6.0900 |
| Phosphorus | 235.500 | 0.004 | 0.0000 | 30.9738 | 1.8200 |
| Sulfur | 281.900 | 0.002 | 0.0000 | 32.0600 | 2.0900 |
| μ Total (1/cm) = 917.8627 | | | μ Total (1/inch) = 2331.3712 | | |

Note: Theta (degrees): 78.201; Density ($g/cm^3$): 7.87.

Depth (Microns)

| PSI = | 0 | 18 | 26 | 32 | 39 | 45 |
|---|---|---|---|---|---|---|
| T = 0.50 | 3.696 | 3.499 | 3.288 | 3.081 | 2.790 | 2.499 |
| T = 0.67 | 5.912 | 5.597 | 5.258 | 4.928 | 4.463 | 3.998 |
| T = 0.95 | 15.974 | 15.122 | 14.209 | 13.316 | 12.059 | 10.803 |

Depth (Mils)

| PSI = | 0 | 18 | 26 | 32 | 39 | 45 |
|---|---|---|---|---|---|---|
| T = 0.50 | 0.146 | 0.138 | 0.129 | 0.121 | 0.110 | 0.098 |
| T = 0.67 | 0.233 | 0.220 | 0.207 | 0.194 | 0.176 | 0.157 |
| T = 0.95 | 0.629 | 0.595 | 0.559 | 0.524 | 0.475 | 0.425 |

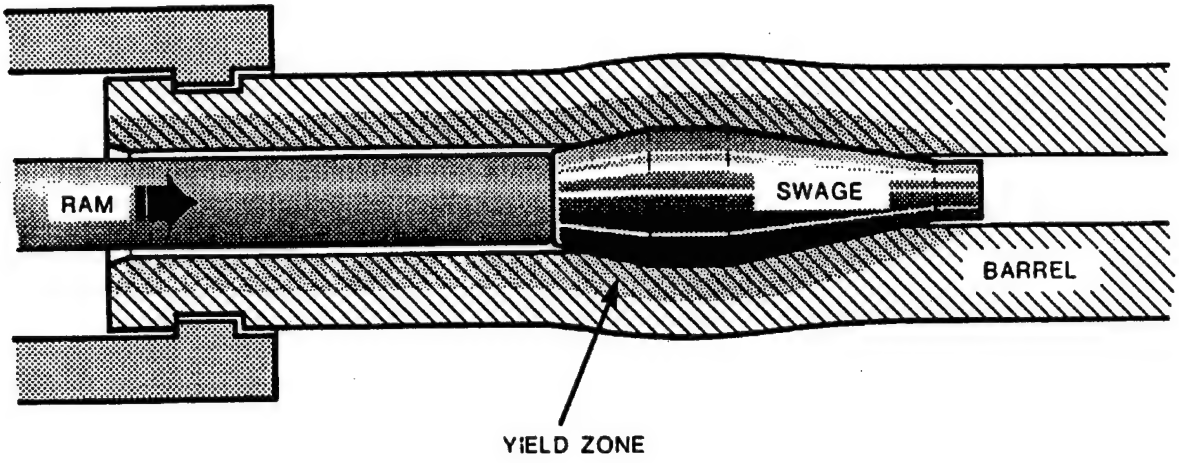


Figure 1a. Swage autofrettage of a cylinder.

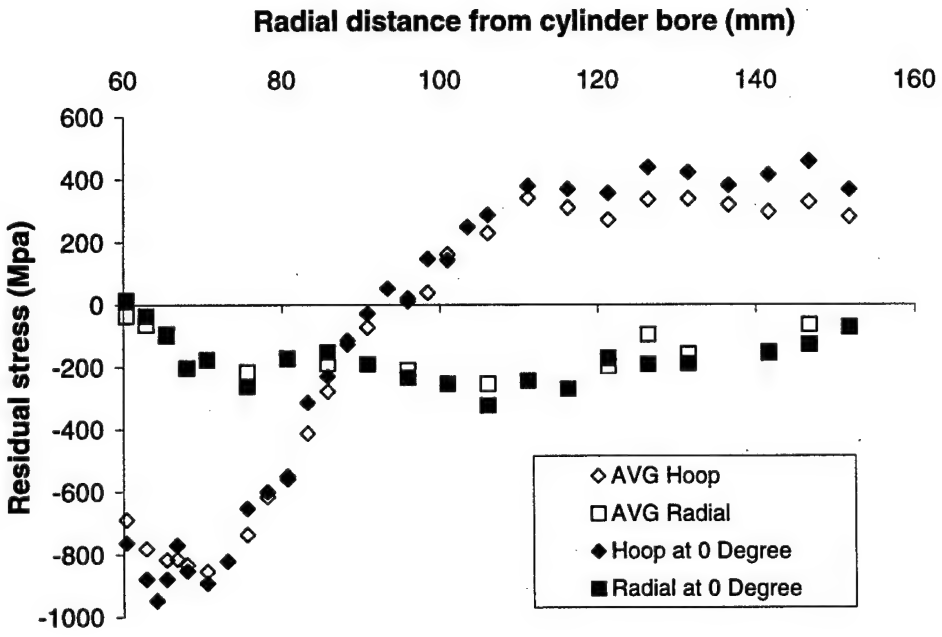


Figure 1b. X-ray hoop and radial residual stress distributions.

FEA Model of 120 mm cylinder
using 20-axisymmetric elements
with 8-nodes each

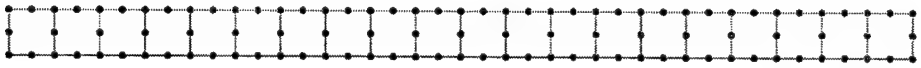

under 100mil internal dilation


Figure 1c. Mesh used in the finite element model.

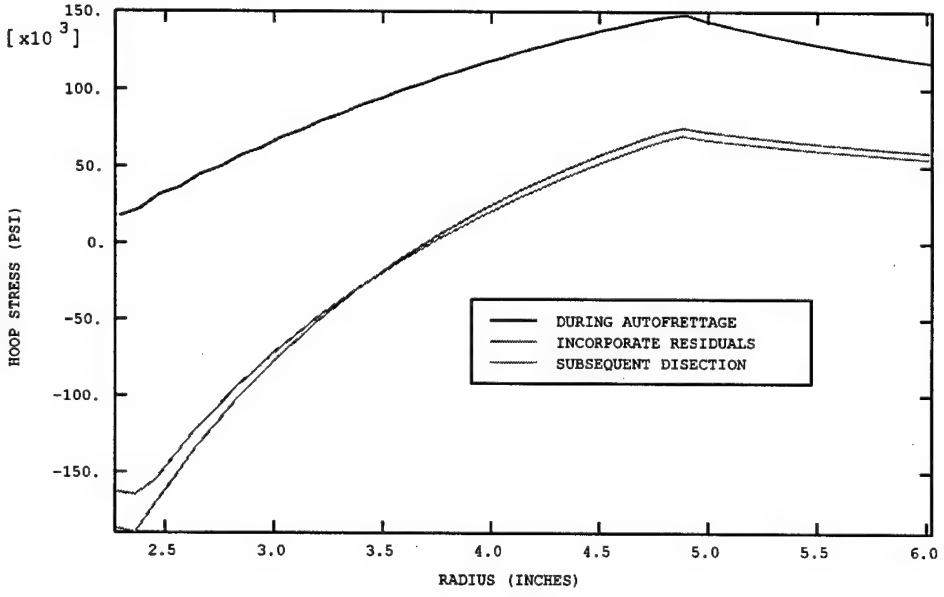


Figure 1d. Hoop stresses before and after applying internal pressure.

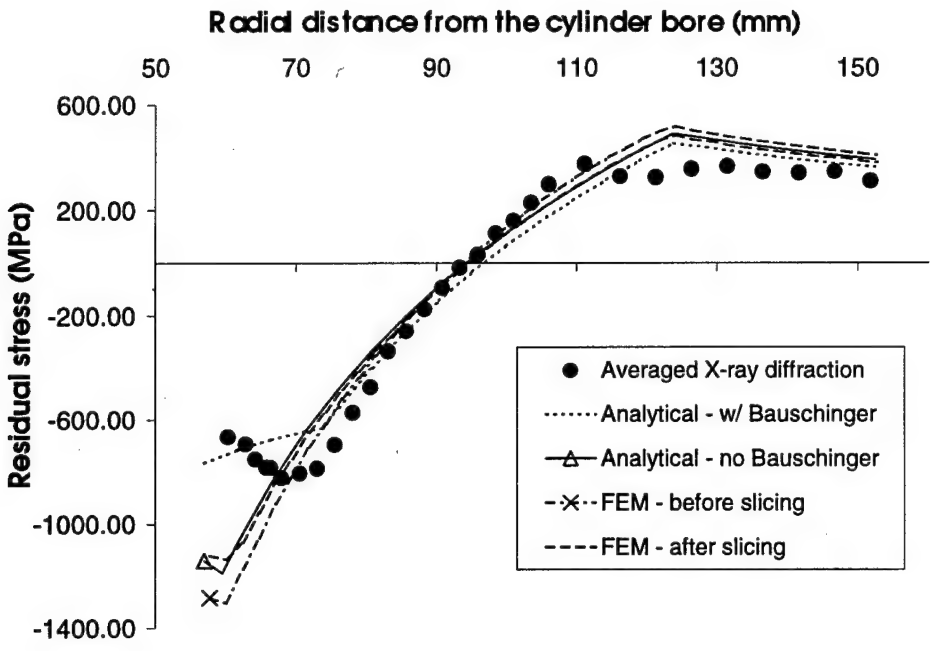


Figure 1e. Finite element and analytical models and experimental hoop stresses.

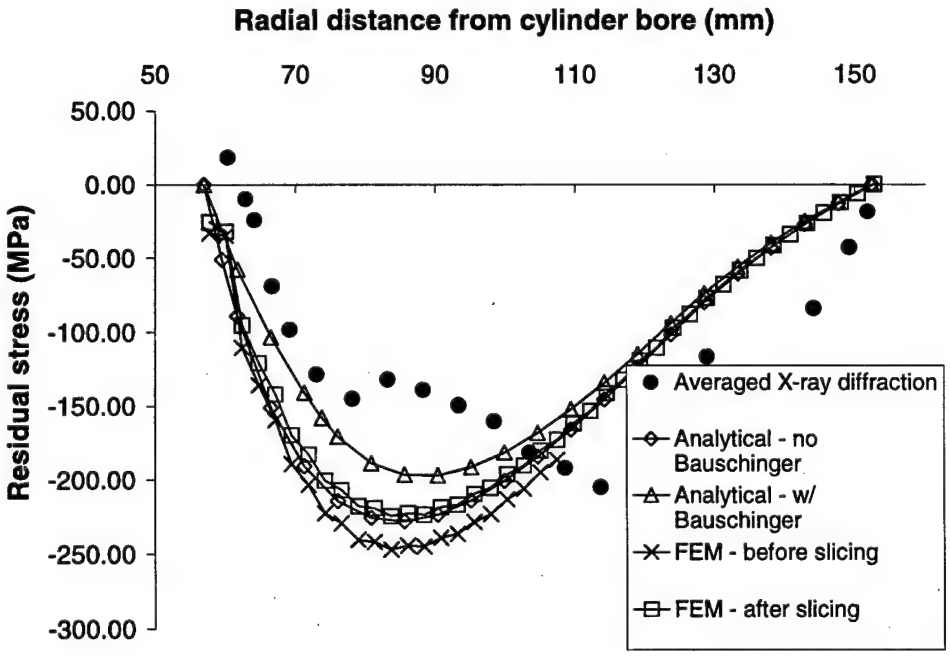


Figure 1f. Finite element and analytical models and experimental radial stresses.

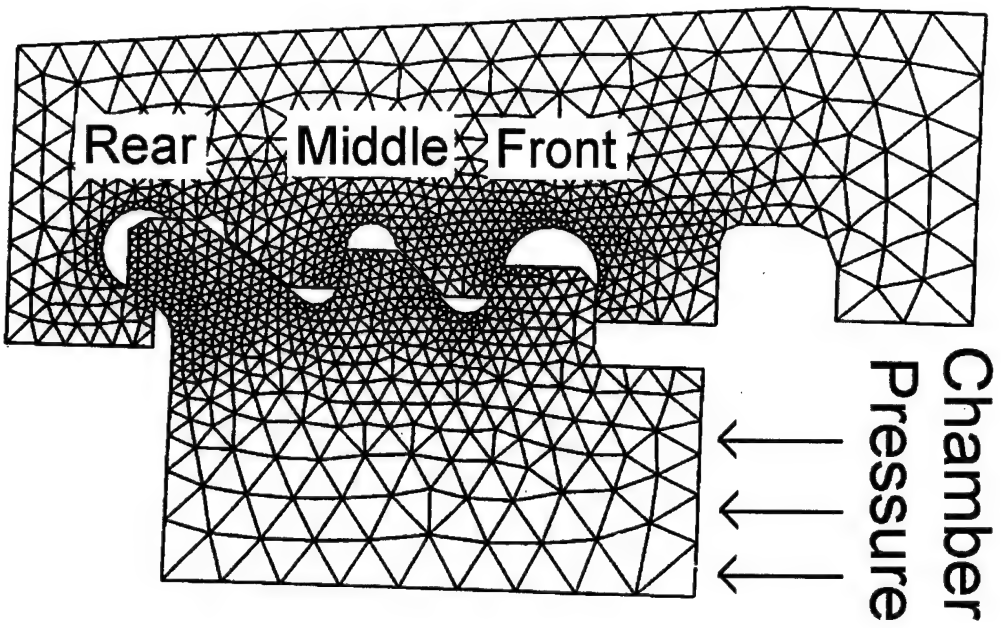


Figure 2a. Multi-lug breech geometry and finite element mesh.

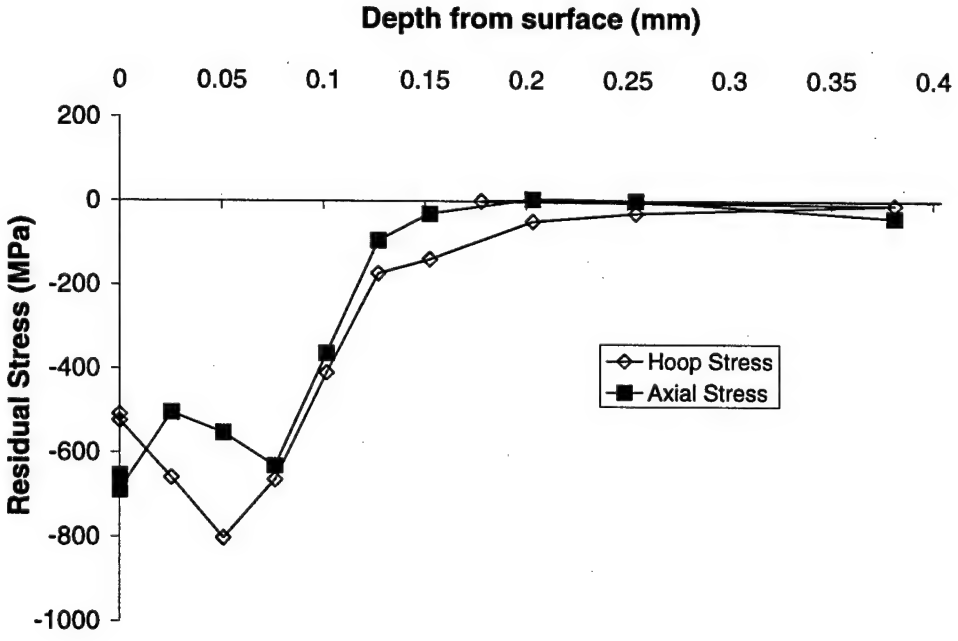


Figure 2b. Hoop and axial shot-peening stresses in the middle lug.

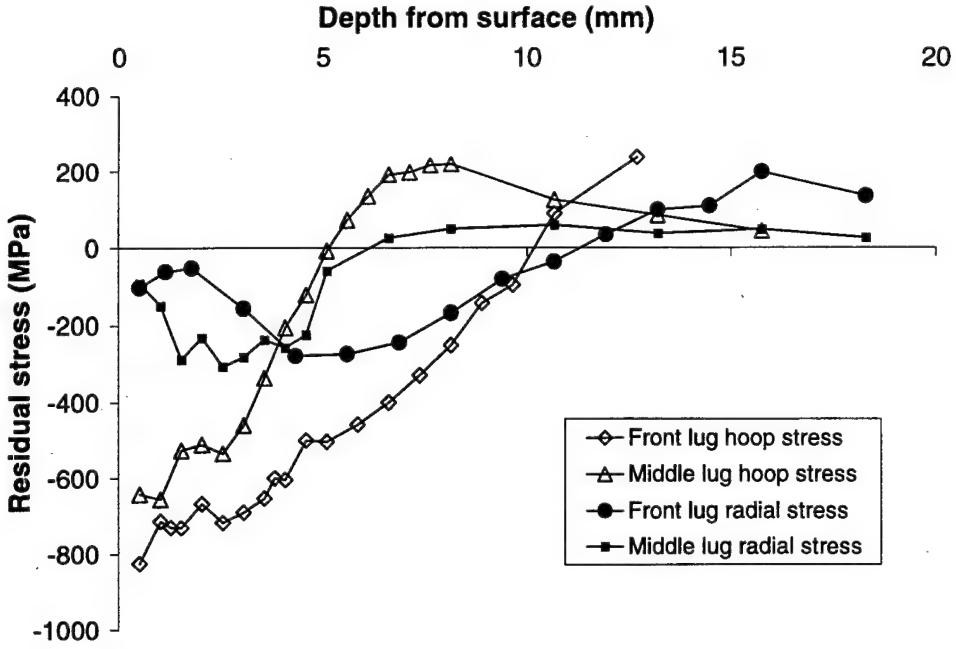


Figure 2c. X-ray hoop and radial stresses in front and middle lugs.

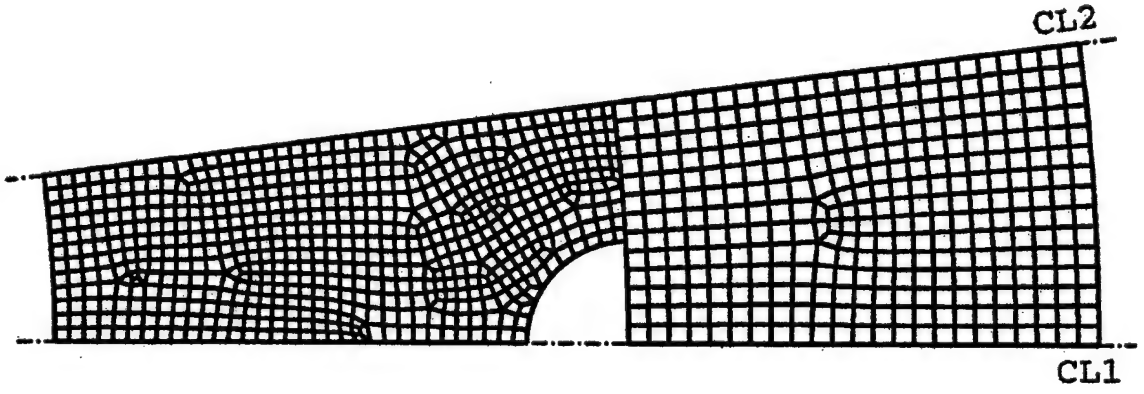


Figure 3a. A slice of the swaged perforated cylinder and finite element mesh.

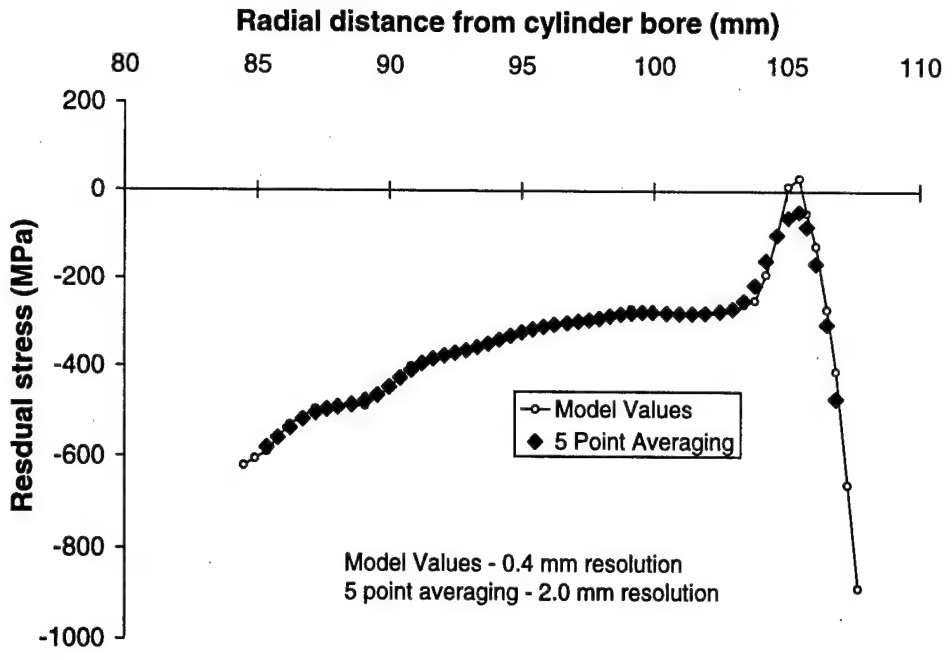


Figure 3b. Finite element hoop stress (60% overstrain) and resolution simulation.

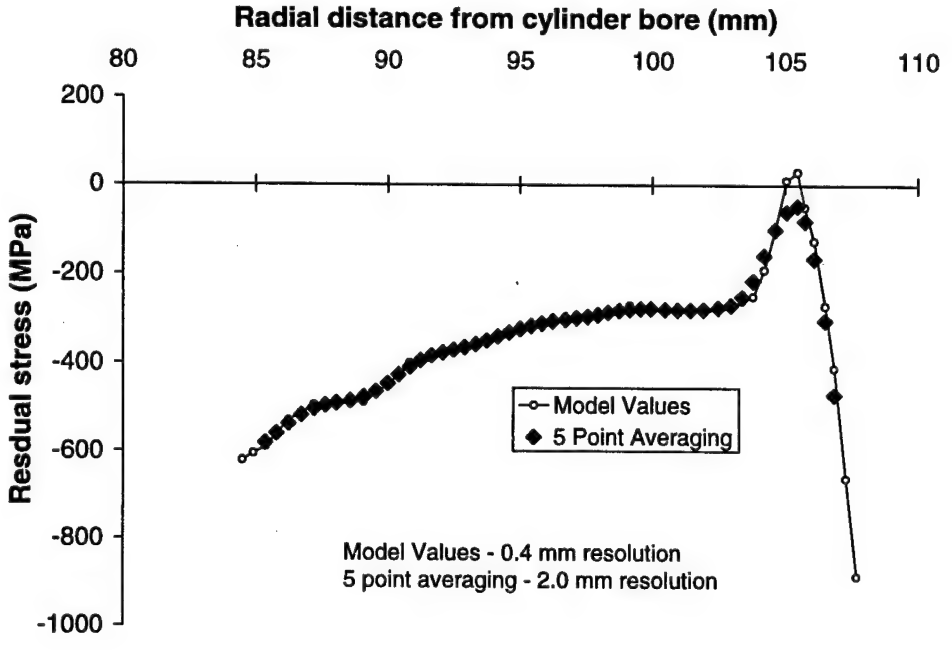


Figure 3c. Hoop stresses in perforated cylinder.

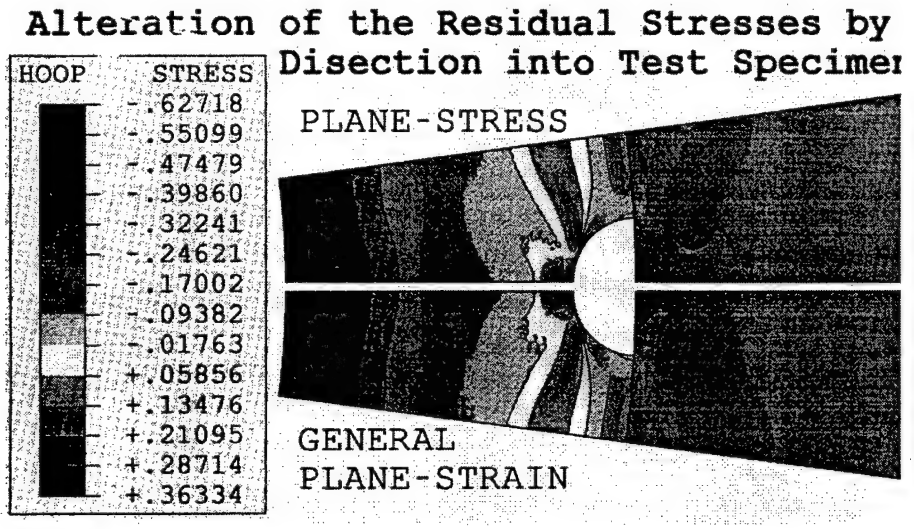


Figure 3d. ABACUS hoop residual stress using plane-stress and generalized plane-strain.

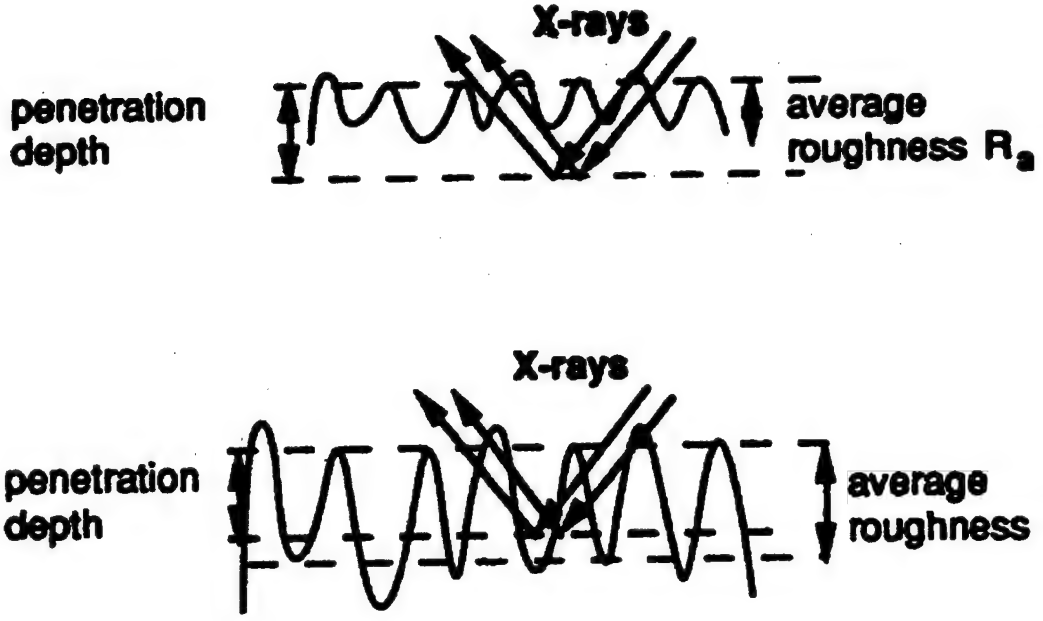


Figure 4a. Roughness effect on x-ray penetration.

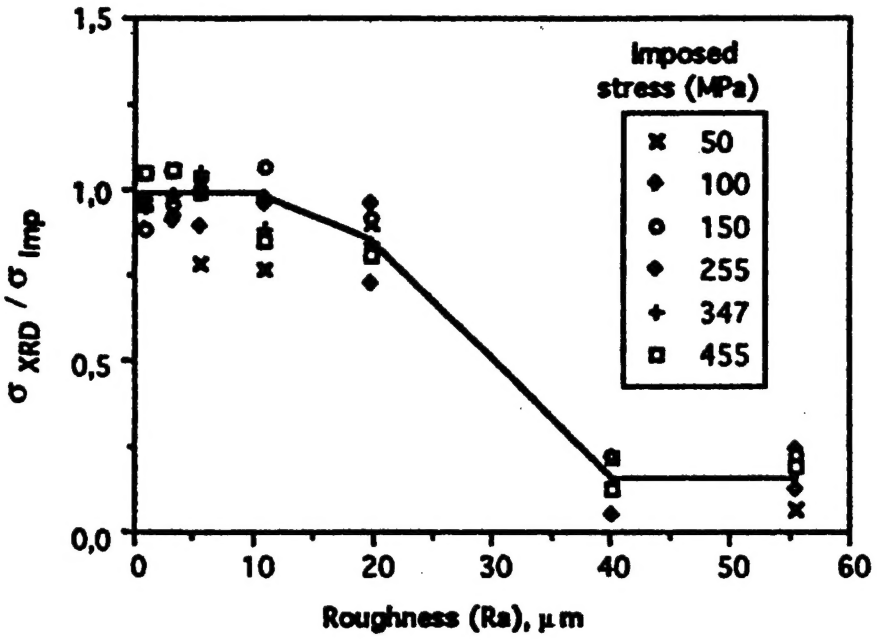


Figure 4b. X-ray residual stress versus roughness.

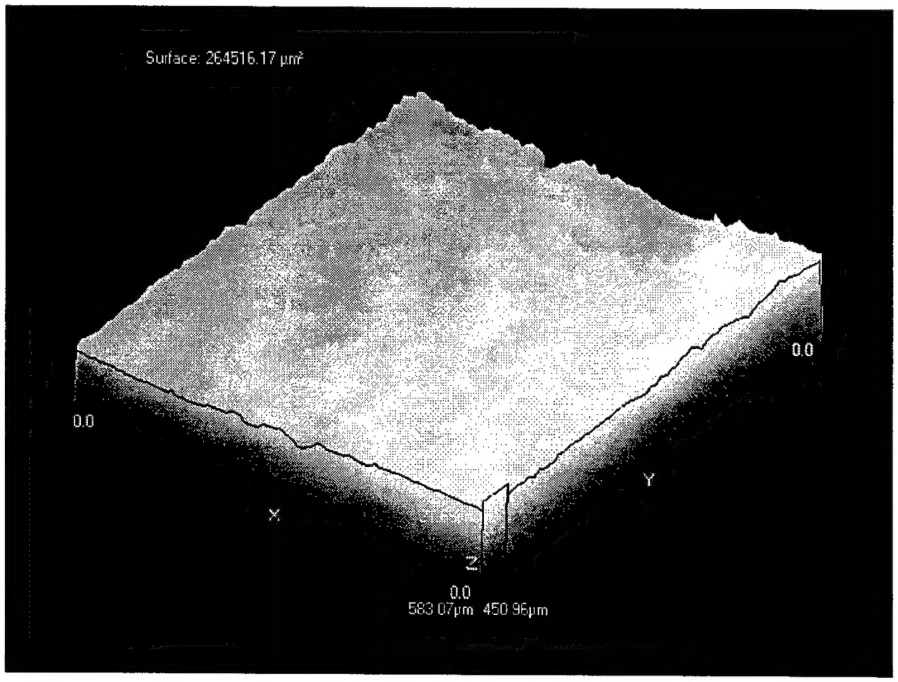


Figure 5a. Steel surface after mild electropolishing using perchloric acid.

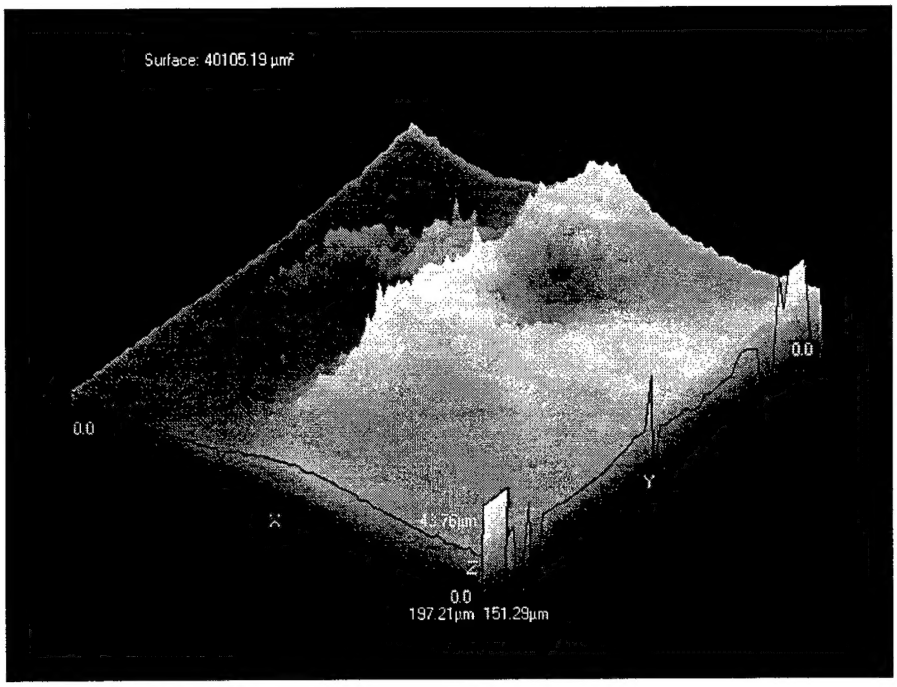


Figure 5b. Steel surface after aggressive etching with HF and hydrogen peroxide mixture.

TECHNICAL REPORT INTERNAL DISTRIBUTION LIST

| | NO. OF COPIES |
|---|---|
| TECHNICAL LIBRARY<br>ATTN: AMSTA-AR-CCB-O | 5 |
| TECHNICAL PUBLICATIONS & EDITING SECTION<br>ATTN: AMSTA-AR-CCB-O | 3 |
| OPERATIONS DIRECTORATE<br>ATTN: SIOWV-ODP-P | 1 |
| DIRECTOR, PROCUREMENT & CONTRACTING DIRECTORATE<br>ATTN: SIOWV-PP | 1 |
| DIRECTOR, PRODUCT ASSURANCE & TEST DIRECTORATE<br>ATTN: SIOWV-QA | 1 |

NOTE: PLEASE NOTIFY DIRECTOR, BENÉT LABORATORIES, ATTN: AMSTA-AR-CCB-O OF ADDRESS CHANGES.

TECHNICAL REPORT EXTERNAL DISTRIBUTION LIST

| | NO. OF COPIES |
|---|---|
| DEFENSE TECHNICAL INFO CENTER<br>ATTN: DTIC-OCA (ACQUISITIONS)<br>8725 JOHN J. KINGMAN ROAD<br>STE 0944<br>FT. BELVOIR, VA 22060-6218 | 2 |
| COMMANDER<br>U.S. ARMY ARDEC<br>ATTN: AMSTA-AR-WEE, BLDG. 3022 | 1 |
| AMSTA-AR-AET-O, BLDG. 183 | 1 |
| AMSTA-AR-FSA, BLDG. 61 | 1 |
| AMSTA-AR-FSX | 1 |
| AMSTA-AR-FSA-M, BLDG. 61 SO | 1 |
| AMSTA-AR-WEL-TL, BLDG. 59<br>PICATINNY ARSENAL, NJ 07806-5000 | 2 |
| DIRECTOR<br>U.S. ARMY RESEARCH LABORATORY<br>ATTN: AMSRL-DD-T, BLDG. 305<br>ABERDEEN PROVING GROUND, MD 21005-5066 | 1 |
| DIRECTOR<br>U.S. ARMY RESEARCH LABORATORY<br>ATTN: AMSRL-WM-MB (DR. B. BURNS)<br>ABERDEEN PROVING GROUND, MD 21005-5066 | 1 |
| COMMANDER<br>U.S. ARMY RESEARCH OFFICE<br>ATTN: TECHNICAL LIBRARIAN<br>P.O. BOX 12211<br>4300 S. MIAMI BOULEVARD<br>RESEARCH TRIANGLE PARK, NC 27709-2211 | 1 |
| COMMANDER<br>ROCK ISLAND ARSENAL<br>ATTN: SIORI-SEM-L<br>ROCK ISLAND, IL 61299-5001 | 1 |
| COMMANDER<br>U.S. ARMY TANK-AUTMV R&D COMMAND<br>ATTN: AMSTA-DDL (TECH LIBRARY)<br>WARREN, MI 48397-5000 | 1 |
| COMMANDER<br>U.S. MILITARY ACADEMY<br>ATTN: DEPT OF CIVIL & MECH ENGR<br>WEST POINT, NY 10966-1792 | 1 |
| U.S. ARMY AVIATION AND MISSILE COM<br>REDSTONE SCIENTIFIC INFO CENTER<br>ATTN: AMSAM-RD-OB-R (DOCUMENTS)<br>REDSTONE ARSENAL, AL 35898-5000 | 2 |
| COMMANDER<br>U.S. ARMY FOREIGN SCI & TECH CENTER<br>ATTN: DRXST-SD<br>220 7TH STREET, N.E.<br>CHARLOTTESVILLE, VA 22901 | 1 |

NOTE: PLEASE NOTIFY COMMANDER, ARMAMENT RESEARCH, DEVELOPMENT, AND ENGINEERING CENTER, BENÉT LABORATORIES, CCAC, U.S. ARMY TANK-AUTOMOTIVE AND ARMAMENTS COMMAND, AMSTA-AR-CCB-O, WATERVLIET, NY 12189-4050 OF ADDRESS CHANGES.